J. theor. Biol. (1998) **194,** 551–559
Article No. jt980774

Hysteresis in Force Probe Measurements: a Dynamical Systems Perspective

BRUCE E. SHAPIRO*† AND HONG QIAN‡

**Department of Biomathematics*, *UCLA School of Medicine*, *AV*-155 *CHS*, 10833 *Le Conte Ave*, *Los Angeles*, *CA* 90095-1766, *U.S.A.* and
‡*Department of Applied Mathematics and Bioengineering*, *University of Washington*, *Seattle*, *WA* 98195-2420, *U.S.A.*

(*Received on* 21 *January* 1998, *Accepted in revised form on* 23 *June* 1998)

Macromolecular binding forces between single protein-ligand pairs have been directly measured with the Atomic Force Microscope (AFM) in several recent experiments. In a typical measurement, the AFM probe, or cantilever, is attached to the ligand and exerts a disruptive force on the bond between the macromolecular pair while the receptor is held fixed; the probe is then moved away from the substrate until the bond is broken. When the bond actually breaks, the tip is observed to slip; in fact, the ligand is jumping to a new equilibrium point determined purely by the cantilever, as if the receptor had been instantaneously moved to infinity. This "jumping-off" or "minimum rupture force" is determined by measuring cantilever deflection. In a similar manner, the two molecules can be brought together and the "jumping-on" force can be determined. These two measurements will result in different estimates of the binding force due to hysteresis. This hysteresis is caused by a cusp catastrophe in the space defined by probe position and cantilever stiffness. The phenomena of "jumping-off" in macromolecular rupture experiments and "jumping-on" when molecules are brought together occur when the system passes through a saddle-node bifurcation as the probe position is varied. Probe approach and withdrawal result in different post-bifurcation equilibria, different energy dissipation, and different force measurements.

1. Introduction

Forces between and within individual biomolecules have been directly measured in aqueous solution in recent experiments. For example, the atomic force microscope (AFM) has been used to study such entities as the binding forces between single protein-ligand pairs (Florin *et al.*, 1994; Moy *et al.*, 1994), hydrogen bonds between DNA base-pairs (Boland & Ratner, 1995), and the interaction between complementary strands of DNA (Lee *et al.*, 1994; Florin *et al.*, 1995). More recently, the reversible unfolding of proteins has also been examined with the AFM (Rief *et al.*, 1997) and laser tweezers (Kellermayer *et al.*, 1997; Tskhovrebova *et al.*, 1997). Hysteresis, in which the observed force depends on the direction of probe motion, is an inherent property of such measurements. Hence great care must be taken in the interpretation of these experimental results. While the present analysis will focus on

†Author to whom correspondence should be addressed. E-mail: bshapiro@ucla.edu

0022–5193/98/020551 + 09 $30.00/0

ligand-receptor separation with the AFM, it is equally valid for other types of force probes, such as optical trapping (Block, 1995; Kuo & Sheetz, 1993), reflection interference microscopy (Evans *et al*., 1995; Evans, 1996), flexible glass fibers (Meyerhofer & Howard, 1995), and magnetic beads (Smith *et al*., 1992).

In a typical measurement, the AFM probe is attached to a ligand and brought into proximity of the receptor, which is held fixed. When the molecular pair join together, the tip is observed to "slip" ("jumping-on"). During withdrawal, the probe, still attached to the ligand, exerts a disruptive force on the bond holding the pair together, and is withdrawn until the bond is broken ("jumping-off"), also observed as a "slip." The observed "jumping-on" and "jumping-off" forces are different due to the phenomenon of hysteresis. The random thermal forces due to the Brownian motion of a particle in aqueous solution make this an inherently stochastic problem. However, the resulting equations are complicated and obscure the underlying physics. Thus the following question naturally arises: how valid is a classical dynamical approach? Can the problem be interpreted using the methods of nonlinear dynamics? If so, then what do the force measurements actually represent, and why does hysteresis occur? While this question has been theoretically addressed in terms of tip–surface interactions (Pethica & Olver, 1987), no rigorous mathematical description of the hysteresis utilizing the methods of nonlinear dynamics has been previously published.

2. Method

Jumping, which is an irreversible thermodynamic process in which energy is dissipated via viscous damping, can be easily understood with the methods of nonlinear dynamics. In a one-dimensional model the molecules can be treated as simple point masses. Receptor position is fixed, ligand motion is constrained to a single axis, and center-of-mass effects and off-axis forces are ignored. The cantilever is a simple harmonic oscillator (spring constant k, probe position d) and the intermolecular force is a function $F(x)$ of ligand-receptor separation (equilibrium separation x_0). For any fixed value of d

$$m\ddot{x} = -\eta\dot{x} + F(x) - k(x - d) \tag{1}$$

where m is the mass of the ligand. The frictional term $(-\eta\dot{x})$ is included because biomolecules are typically suspended in a fluid of viscosity ξ (where $\eta \approx 6\pi r\xi$). For water, $\xi \approx 0.01$ poise ($\eta \approx 3.8 \times 10^{-11}$ kg/s) (McQuarrie, 1976, p. 452). "Jumping-off" occurs when a force barrier described by the function $F(x)$ is penetrated as d is increased. When the probe is moving d is not constant; treating d as a control parameter gives an infinitely slowly moving probe approximation, which we consider first. The exact solution requires treating d as a function of time. The resulting differential equation is non-autonomous.

Specific calculations are considerably simplified if the exact form of $F(x)$ is known, especially if there is some potential function V such that

$$F(x) = -\nabla V(x) \tag{2}$$

Intermolecular potentials are typically spoon-shaped; in other words, $\lim_{x \to 0} V(x) = \infty$, $\lim_{x \to \infty} V(x) = 0$, and there is a stable global minimum value at some x^* (corresponding to the equilibrium intermolecular separation), where $0 < x^* < \infty$. A commonly used form for V is the Lennard-Jones 6–12 potential (Sarid, 1991) which is illustrated in Fig. 1.

$$V_{LJ} = V_0\left[\left(\frac{x_0}{x}\right)^{12} - 2\left(\frac{x_0}{x}\right)^{6}\right] \tag{3}$$

Results obtained using the Lennard-Jones potential are indicated with the subscript LJ in the remainder of this paper. A total potential

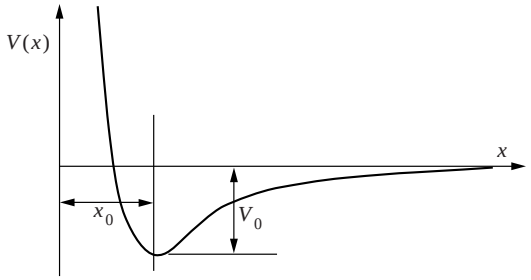

FIG. 1. The Lennard-Jones 6–12 potential given by eqn (3).

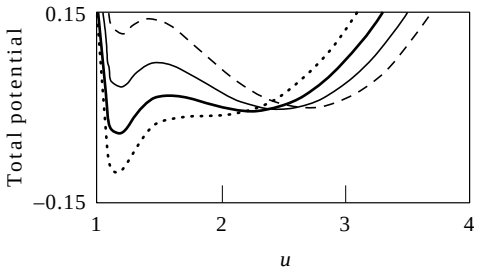

FIG. 2. Total potential function [sum of intermolecular and probe potentials, eqn (6)] during probe approach with a Lennard-Jones 6–12 potential. The probe is brought in from $d = 2.7$ (dashed line), through $d = 2.5$ (solid line) and $d = 2.3$ (bold line) to $d = 2.1$ (dotted line), where there is no barrier and "jumping-on" occurs. The dimensionless abscissa is in units of x/x_0, and the ordinate is V/V_0. A spring constant of $k = 0.3V_0/x_0^2$ is used.

function, consisting of the sum of the intermolecular and probe elastic potentials, can then be defined as

$$\varepsilon(x) = V(x) + \frac{1}{2}k(x - d)^2 \tag{4}$$

Substituting eqns (2) and (4) into eqn (1) gives the revised dynamical equation as

$$m\ddot{x} + \eta\dot{x} = -\nabla\varepsilon(x) \tag{5}$$

$\varepsilon(x)$ has two wells, one each for the probe and intermolecular forces. From eqns (3) and (4) the total potential for a Lennard-Jones 6–12 interaction is

$$\varepsilon_{LJ}(x) = V_0\left[\left(\frac{x_0}{x}\right)^{12} - 2\left(\frac{x_0}{x}\right)^{6}\right] + \tfrac{1}{2}k(x - d)^2 \tag{6}$$

During probe approach (Fig. 2), the probe well shrinks while the intermolecular well grows; the opposite occurs during withdrawal (Fig. 3).

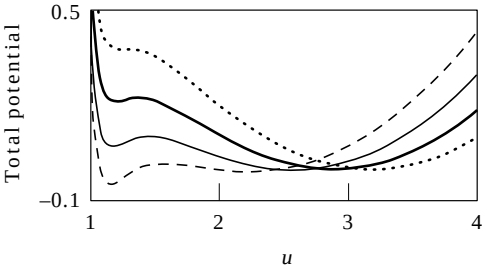

FIG. 3. Reversal of the simulation illustrated in Fig. 2 with the same parameter values. The probe starts at $d = 2.3$ (dashed line), moves through $d = 2.6$ (solid line) and $d = 2.9$ (bold line) to $d = 3.1$ (dotted line) when the barrier falls and "jumping-off" occurs.

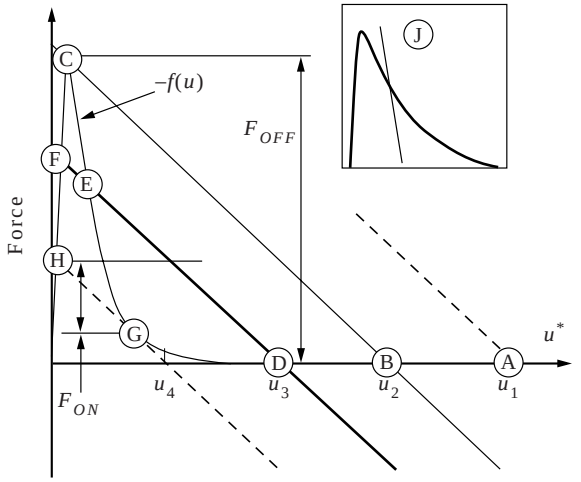

FIG. 4. Graphical illustration of hysteresis. The smooth curve represents the intermolecular force [right hand side of eqn (15)]. The lines illustrate the probe force [left hand side of eqn (15)] at four different probe locations (dashed line $d = u_1$; solid line $d = u_2$; bold line $d = u_3$; bold dashes $d = u_4$, where $u_1 > u_2 > u_3 > u_4$). Attractive (negative) forces are represented by the ordinate. The origin of the abscissa is at $u^* = 1$. Inward motion of the probe corresponds to moving the lines to the left in the figure, and outward motion corresponds to moving the lines to the right. Fixed points occur at intersections of $f(u)$ and the lines for probe potential (illustrated by points A–H). During approach, there is one fixed point (A), for $d > u_2$, then two (B and C, at $d = u_2$), and finally three fixed points (D, E, and F, $u_4 < d < u_2$). The fixed point C splits into fixed points E and F at $d = u_2$; points D and E coalesce into G at $d = u_4$. In the infinitely slow probe approximation the system follows ABDG; further inward motion causes a jump to point H from point G. The "jumping on" force, F_{ON}, is the force difference of this jump. When the experiment is reversed, starting at H (withdrawal), the system follows HFCBA. A much larger "jumping-off" force $F_{OFF} > F_{ON}$ is observed in the jump from C to B than in the jump from H to G during inward probe motion. Notice that the force curve between C and G is never observed. In the example illustrated in the inset (J), the probe is so stiff that there is always exactly one steady state. Compare this and Fig. 5 with Figs 1.4(a) and 1.5 of Murray (1993, pp. 6–7).

When one well disappears, the ligand "falls" into the other well; this is referred to as "jumping-on" (in adhesion experiments) or "jumping-off" (in rupture experiments). The distance which the ligand must "fall" is substantially larger during "jumping-off" then during "jumping-on" as illustrated in Figs 2–4.

The process of non-dimensionalization allows one to extract a minimal set of fundamental physical parameters corresponding to non-dimensionalizations α, β, and D of the viscosity, spring constant, and probe position. Although well depth, V_0, and equilibrium intermolecular

separation x_0 could also be considered as parameters, for any particular macromolecular complex, they are fixed (in the present model). Furthermore, since α (viscosity) and β (stiffness) are fixed during any given experiment, the cantilever position, D, becomes the principal control parameter.

The spatial dependence can be expressed in terms of the equilibrium intermolecular spacing x_0. Thus we take $u = x/x_0$ as the dimensionless spatial variable and $D = d/x_0$ as the dimensionless probe position. There is no obvious characteristic time for the system, so we must construct one. We arbitrarily select any characteristic force value F_0 (e.g. $F_{0,LJ} = V_0/x_0$) and use it to construct a time constant $\tau = \sqrt{mx_0/F_0}$ [e.g. $\tau_{LJ} = x_0\sqrt{m/V_0}$]. Then we can define our time variable let $T = t/\tau$, and a dimensionless force function as $f(u) = F(ux_0)/F_0$. The dimensionless Lennard-Jones 6–12 force is

$$f_{LJ}(u) = 12(u^{-13} - u^{-7}) \tag{7}$$

Define $\alpha = \eta\tau/m$ as the dimensionless friction and $\beta = \omega^2\tau^2 = k\tau^2/m$ as the dimensionless stiffness, where $\omega = \sqrt{k/m}$ is the probe's natural harmonic frequency. Then the dimensionless form of eqn (1) is

$$u'' = -\alpha u' + f(u) - \beta(u - D) \tag{8}$$

where $u' = \mathrm{d}u/\mathrm{d}T$. Typical parameter values for a system in aqueous solution are $\omega \approx 156$ GHz, $\tau \approx 0.267$ ps, $\beta \approx 0.00174$ and $\alpha \approx 4.0$ for $m = 150$ Dalton, $x_0 = 2$Å, $V_0 = 20$ kcal/mole and $k = 0.006$ N/m (Florin *et al.*, 1994). Commercial AFM cantilevers have $0.01\ \mathrm{N/m} \leqslant k \leqslant 30$ N/m. Recent force measurements have been reported using k as high as 0.6 N/m ($\beta \approx 0.17$) (Kasas *et al.*, 1997).

The first order system equivalent to eqn (8) is

$$\mathrm{d}u/\mathrm{d}T = v \tag{9}$$

$$\mathrm{d}v/\mathrm{d}T = -\alpha v + f(u) - \beta(u - D). \tag{10}$$

The Jacobian, which is of interest at the fixed points, is

$$J = \begin{bmatrix} 0 & 1 \\ \nabla_u f - \beta & -\alpha \end{bmatrix} \tag{11}$$

and has eigenvalues

$$\lambda = -\frac{\alpha}{2} \pm \frac{1}{2}\sqrt{\alpha^2 + 4(\nabla_u f - \beta)} \tag{12}$$

or

$$\lambda_{LJ} = -\frac{\alpha}{2} \pm \frac{1}{2}\sqrt{\alpha^2 + 4(-156u^{-14} + 84u^{-8} - \beta)} \tag{13}$$

for the Lennard-Jones potential. Fixed points (u^*, v^*) occur at the bottom of the two potential wells and the top of the barrier between them. From eqns (9) and (10),

$$v^* = 0 \tag{14}$$

and

$$\beta(u^* - D) = f(u^*). \tag{15}$$

Fixed points with the Lennard-Jones potential are found by combining eqns (7) and (15),

$$\beta(u^*_{LJ})^{14} - \beta(u^*_{LJ})^{13}D + 12(u^*_{LJ})^6 - 12 = 0. \tag{16}$$

Three fixed points must exist for the force observations to be made, as illustrated in Fig. 4. In this figure, straight lines represent the left hand side of eqn (15), and a smooth curve the right hand side; fixed points occur at the intersections of the lines with the curve. This leads to a constraint on the stiffness of the cantilever, described by the parameter β. For extremely stiff springs the line representing the probe force is always steeper than the steepest part of the curve representing the intermolecular force, only one root exists, and the AFM will never slip.

The locus of fixed points expressed as a function of the parameters β and D, $u^*_{LJ}(\beta,D)$, is a two-dimensional surface which partially "folds" back on itself, as illustrated in Fig. 5. The projection of the "folds" [defined as points where a tangent plane to $u^*_{LJ}(\beta,D)$ is vertical] into the (β, D) plane is a cusp-shaped curve whose interior contains the points for which three fixed points exist. The point of the cusp occurs at $\beta = \beta_{\max}$, where $\beta_{\max}$ is determined from the value $\hat{u}$ such that the slope of the force curve at $\hat{u}$, $f'(\hat{u})$,

is maximized; then $\beta_{\max} = f'(\hat{u})$. For V_{LJ}, the probe is "too-stiff" unless

$$\beta < \beta_{\max,LJ} = (144/13) \times (13/4)^{-1/3} \approx 7.48.$$

This limitation does not pose a problem for the AFM, where β is typically one to three orders of magnitude smaller; however, it should be kept in mind as newer force probe techniques are developed. With softer springs, force measurements are possible, although the entire force curve will never be observable.

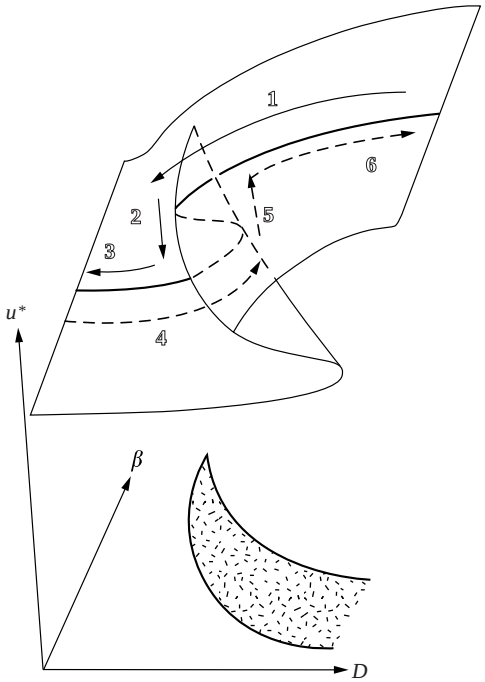

FIG. 5. Points on the surface correspond to the locations of the fixed points for any given parameter values β and D. The surface partially folds back over itself, revealing a cusp-shaped region in the parameter space (shaded) within which there are exactly three fixed points. A plane perpendicular to the β-axis which passes through the cusp intersects the surface in an S-shaped curve. This is the bifurcation curve. During any single experiment, β (cantilever stiffness) is fixed and the state of the system is constrained to remain on this curve. Hysteresis occurs because of the fold in the surface, which causes the system to "fall" from the upper to the lower surface during probe approach, and "jump" from the lower to the upper surface during probe withdrawal. As the ligand is brought in from infinity (solid arrows) it follows the upper leg of the bifurcation curve until it can do no further (1), "falling" over the edge to the bottom leg (2) as it forced further inward (3). When the probe is withdrawn [(4), dashed arrows], the ligand can continue beyond the earlier bifurcation point until the lower leg of the S-curve twists back on itself (5). Forcing D to increase causes the system to "jump" up to the higher curve (6). Hence the process is not reversible.

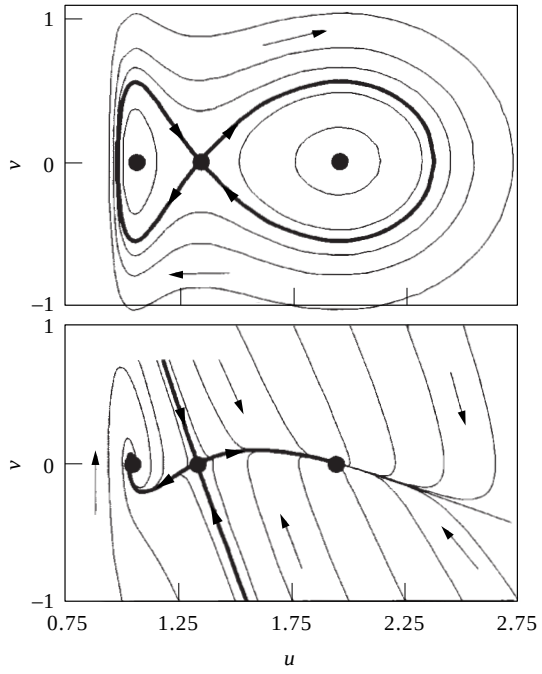

FIG. 6. Phase portrait for force probe measurement. Top: $\alpha = 0$ (vacuum); Bottom: $\alpha = 4$ (aqueous solution). The fixed points are indicated by the solid circles, and their stable and unstable manifolds by the bold lines.

3. Results

3.1. IN VACUUM

Consider first the vacuum case ($\alpha = 0$). When

$$\nabla_u f = -156u^{-14} + 84u^{-8} < \beta$$

λ is purely imaginary and fixed points which satisfy this condition are surrounded by closed trajectories (top plot of Fig. 6, numerical simulation). These are the orbits of ligands bound to the receptor or to the probe. When

$$\nabla_u f = -156u^{-14} + 84u^{-8} > \beta$$

the eigenvalues are a positive/negative pair. Fixed points are saddle nodes, which occur when the probe and intermolecular force are exactly balanced, and the ligand "sits" atop the barrier. Any perturbation of the ligand's position causes

it to "fall" into one or the other of the two wells. Finally, when

$$\nabla_u f = \beta$$

the eigenvalues are both equal to zero. As D is slowly varied the locations of the fixed points in u will change, causing $(\nabla_u f - \beta)$ to change signs as the system passes through a saddle-node bifurcation.

This bifurcation allows for hysteresis to occur in force measurements. In macromolecular separation, there are initially three fixed points. Those at well-bottoms have imaginary eigenvalues, while the one at the peak has a positive/negative pair. At the exact instant of rupture, there are precisely two points where $V'(x) = 0$: the probe well, and a saddle-node formed by the coalescence of the macromolecular well and the barrier. Any positive increase in D causes this fixed point to disappear and the ligand "falls" into the probe well. The situation is reversed when the probe approaches the base, with two critical differences: (1) it is the probe well that coalesces with the barrier, and (2) coalescence occurs at different values of D during approach and withdrawal. The situation is phenomenologically identical to the spruce-budworm population model (Ludwig *et al*., 1978) and is related to a set of problems known as a cusp catastrophe (Murray, 1993, pp. 4–8; Nayfeh & Balachandran, 1995, pp. 85–86).

System dynamics for a single apparatus (fixed β) can be represented by plotting the location of the fixed points (u^*) vs. probe position (D). This plot, which corresponds to planar sections through the surface of Fig. 5 perpendicular to the β-axis (Fig. 7), is called a "bifurcation diagram." A bifurcation diagram is interpreted as described in Fig. 5. As the ligand is "brought in" from infinity by reducing D, it follows the top leg of the S-shaped curve until it can go no further. Additional reduction in probe position causes the ligand to fall to the lower leg of the S-curve, because it can go no further on the upper leg. When the probe is withdrawn to separate the pair, the ligand follows the lower leg of the S-curve, jumping to the upper leg only when it can follow the bottom one no longer. This type of hysteresis is common around cusp-catastrophes (Nayfeh & Balachandran, 1995, pp. 85–86).

3.2. IN AQUEOUS SOLUTION

Although viscosity does not change the location of the fixed points, the trajectories are significantly different (bottom plot of Fig. 6). When

$$\nabla_u f < \beta - \alpha^2/4$$

the eigenvalues are a complex-conjugate pair with negative real part and the fixed points are stable spirals centers. When

$$\beta - \alpha^2/4 < \nabla_u f < \beta$$

the eigenvalues are both real and negative and the fixed points are nodal attractors. When

$$\nabla_u F = \beta$$

the eigenvalues are $-\alpha$ and 0; the saddle-node bifurcation still occurs as it did in vacuum. When

$$\nabla_u f = \beta - \alpha^2/4$$

both eigenvalues are $-\alpha/2$. This is the transition point between stable spirals and nodal attractors. When

$$\nabla_u f > \beta$$

the eigenvalues are a positive/negative real pair and the nodes are saddle points.

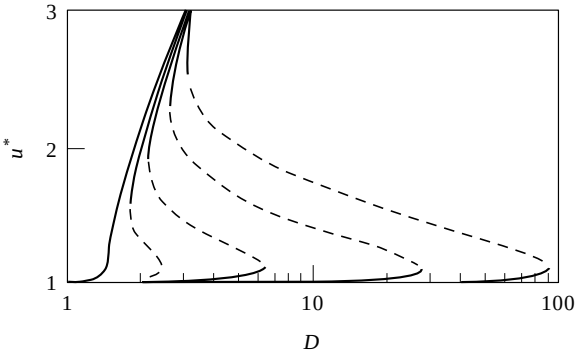

FIG. 7. Bifurcation diagram for various values of β using a Lennard-Jones 6–12 potential. Solid lines correspond to the stable nodes (the wells) and dashed lines to the unstable saddle node (the barrier). Notice that a barrier only exists for a finite range of β; the leftmost curve corresponds to a barrier-free case since $\beta > \beta_{max}$. Left to right, $\beta = 8, 2, 0.5, 0.1, 0.03$.

3.3. MOVING PROBE IN AQUEOUS SOLUTION

If probe motion is taken into account, the system becomes non-autonomous.

$$u'' = -\alpha u' + f(u) - \beta u + \beta D(T)$$

Natural resonances of the system will occur at the poles of the Fourier transform $\hat{u}(\Omega)$ of $u(T)$, where

$$\hat{u}(\Omega) = \hat{h}(\Omega)[\mathscr{F}(\Omega) + \beta\hat{D}(\Omega)]$$

Here $\hat{h}(\Omega) = [\beta + i\alpha\Omega - \Omega^2]^{-1}$ is assumed to be the Fourier transform of some function $h(T)$, and $\mathscr{F}(\Omega)$ and $\hat{D}(\Omega)$ are the Fourier transforms of $f(u(t))$ and $D(T)$, assuming that they exist. Simple poles occur at the zeroes of $\hat{h}(\Omega)$,

$$\Omega = i\frac{\alpha}{2}[1 \pm \sqrt{1 - 4\beta/\alpha^2}]$$

Since it is typically true that $\beta \ll \alpha$, the poles occur approximately at

$$\Omega_1 \approx i\alpha$$

$$\Omega_2 \approx i\beta/\alpha$$

which correspond to frequencies of 14.9 GHz and 1.63 MHz, respectively, using the typical values quoted earlier ($\alpha \approx 4$, $\beta \approx 0.00174$, $\tau \approx 0.267$ ps). Driving the oscillator at either of these frequencies will (mathematically) lead to a Dirac δ-function type of resonance. We can see this formally by inverting the Fourier transform to get

$$u(T) = h(T)*[IFT(\mathscr{F}(\Omega)) + \beta D(T)]$$

where "*" denotes convolution and *IFT* () is the inverse Fourier transform operator. Inversion of h (Ω) contributes a factor of

$$h(T) = \frac{1}{|\Omega_1 - \Omega_2|}[e^{2\pi i\Omega_1 T} + e^{2\pi i\Omega_2 T}]$$

to the convolution, indicating that there will also be a natural resonance at the difference of the first two frequencies, $|\Omega_1 - \Omega_2|$. This third frequency is very close to Ω_1 for the values quoted above. The two exponential terms contribute to the Dirac δ-function resonances.

A second case to consider is where the driving function is linear with time. For example, if the probe in a macromolecular rupture experiment starts at d_0 and moves with a constant velocity c,

$$D(T) = D_0 + CT$$

where $D_0 = d_0/x_0$ and $C = c\tau/x_0$. The resulting dynamics can be understood in terms of the infinitely slow probe, with a third dimension (time) added to the phase space. In vacuum, the closed trajectories gradually spiral out and up along the time axis until they cross the stable manifold of the saddle node corresponding to the instantaneous value of D. This is the "jumping-off" point. From there onward, the trajectories spiral in to the probe well. If the probe velocity is sufficiently high, the trajectories will be monotonic in u but will oscillate in v, even when the system is initially in equilibrium. For slower velocity and lower viscosity u may also oscillate (numerical result, Fig. 8). There is little oscillation at higher viscosities (e.g. water, $\alpha \approx 4$).

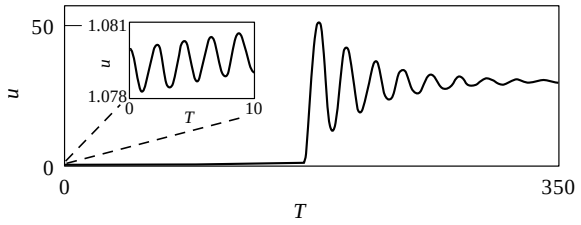

FIG. 8. Oscillation of ligand during AFM probe withdrawal. The probe starts at $u = 1.08$, $v = 0$. Parameter values: $\alpha = 0.05$, $\beta = 0.1$, $c = 5\ \mathrm{ms}^{-1}$.

3.4. STOCHASTIC EFFECTS

Brownian motion of the fluid particles introduces random stochastic forces upon the macromolecules which give a finite probability for "jumping-on" or "jumping-off" while the barrier still exists. In a typical experiment, a large number of measurements are made and a histogram of force-vs.-distance ("force spectrum") is obtained which gives this probability distribution (Florin *et al*., 1994; Moy *et al*., 1994). This probability has been previously determined (Shapiro & Qian, 1997; Evans & Ritchie, 1997) by solving the appropriate Fokker–Planck equation (Chandresekhar, 1943) with Kramers' theory of molecular dissociation (Kramers, 1941). The scope of the present analysis has been limited to a deterministic

analysis of the problem of macromolecular separation. Thus the results presented here would describe the separation of a single macromolecular pair under the influence of an average viscous force, rather than the probability for rupture from a specific geometry. In our previous stochastic analysis (Shapiro & Qian, 1997), we assumed that a probability could be calculated at each *fixed* position of the probe (infinitely slow probe approximation). The stochastic analysis showed that there is a minimum force value, below which rupture is impossible and above which there is a finite possibility of rupture. This force was defined as the "minimum rupture force," which occurs at the one energy-well to two energy-well transition. The probability density function $p(d)$ for "jumping-off" was shown to be

$$p(d) = \frac{\kappa(d)}{V} \exp\left\{ - \int_{x_0}^{d} \frac{\kappa(x)}{V} \, \mathrm{d}x \right\}$$

where

$$\kappa(d) = \frac{\omega_R(d)}{2\pi} \, \mathrm{e}^{-E/kT} \times \left\{ \sqrt{1 + (\eta/2m\omega_B(d))^2} - (\eta/2m\omega_B(d)) \right\}$$

is the rate constant for the reaction

$$\text{Bound Protein} - \text{Ligand Pair} \xrightarrow{\kappa(d)} \text{Unbound Protein} - \text{Ligand Pair}$$

and $\omega_R(d)$ and $\omega_B(d)$ are determined from Taylor expansions of the potential about the reactant well and activation barriers when the cantilever is at position d. Numerical integration of this result gives a bell-shaped curve whose mean and width are a function of probe velocity, with the distribution widening and moving to the right as velocity increases. At very high velocity, the distribution width decreases somewhat, because less time is spent in the stochastic two-well region. In the low velocity limit, the distribution approaches an exponential with a peak at the "minimum rupture force," the expected result for a Poisson process. Oscillations induced by probe motion encountered in the present paper should increase the spread in the force spectrum.

4. Discussion

Our results show that a deterministic analysis can provide a description of the underlying physics *even though the problem is inherently stochastic*. The observed binding force depends upon the position, speed, and direction of probe motion, as well as cantilever stiffness. The force measurements represent the difference between two points on the force-vs.-distance curve. Ideally, these two points represent the natural bound state and the unbound state, where there is no interaction. However, if the cantilever is too stiff, no force observations are possible (Fig. 4). Hence parts of the force-vs.-distance curve are unobservable. Furthermore, adhesion observations give significantly smaller force values than rupture observations because the interaction between the enzyme and the ligand begin before the barrier drops. Thus care must be taken in using expressions like "binding force." Hysteresis occurs because there is a cusp-catastrophe in phase space. Physically, the "slip" or "jumping-off" process is an irreversible thermodynamic process in which energy is dissipated via viscous damping. Mathematically, the state of the system passes through a saddle-node bifurcation as the cantilever position varies where it jumps to a new equilibrium position. A moving probe induces oscillations in the system, causing a spread in the force observations; except at extremely high speed, viscosity damps these oscillations.

The class of experimental techniques analysed in this paper has also been used to stretch and relax long polymers such as Titin, revealing a saw-tooth shaped force spectrum (Rief *et al*., 1997; Kellermayer *et al*., 1997; Tskhovrebova *et al*., 1997). In this case the hysteresis originates from multiple sources, as sub-domains may stretch and relax in different orders. This phenomenon is more pronounced the greater the extension. If high external forces are applied and the rate at which the molecule is stretched or released exceeds the rate of unfolding and refolding of the molecule at equilibrium, a large hysteresis is observed. This process of polymer stretching and releasing should also be explicable by the methods described above and in the previous paper (Shapiro & Qian, 1997),

particularly the graphical explanation (Fig. 4) for force-hysteresis. The only differences would be an increase in the number of energy wells; as the molecule is stretched, individual wells collapse together, while others develop. The state of such a system could jump in a seemingly combinatoric fashion between these wells with a spread determined by the effects of Brownian motion, probe velocity, and stiffness. However, the number of allowed jumps would be limited by the direction of probe motion and the detailed local interactions of the individual molecules in the chain. Thus it should be possible to qualitatively describe the basic physics of stretching protein polymers by combining the methods of nonlinear dynamics with an appropriate Fokker–Planck equation for a model system. This approach generalizes the Zimm–Rouse bead–spring polymer theory (Rouse, 1953; Zimm, 1956).

REFERENCES

Block, S. M. (1995). Nanometers and piconewtons: the macromolecular mechanics of kinesin. *Trends Cell. Biol.* **5,** 169–175.

Boland, T. & Ratner, B. D. (1995). Direct measurement of hydrogen bonding in DNA nucleotide bases by atomic force microscopy. *Proc. Natl. Acad. Sci. U.S.A.* **92,** 5297–5301.

Chandresekhar, S. (1943). Stochastic problems in physics and astronomy. *Rev. Mod. Phys.* **15,** 1–89.

Evans, E. (1996). Dynamic force spectroscopy of weak adhesive bonds. *Bull. Am. Phys. Soc.* **41,** 457.

Evans, E. & Ritchie, J. (1997). Dynamic strength of molecular adhesion bonds. *Biophysical J.* **72,** 1541–1555.

Evans, E., Ritchie, K. & Merkel, K. (1995). Sensitive force technique to probe molecular adhesion and structural linkages at biological interfaces. *Biophysical J.* **68,** 2580–2587.

Florin, E. L., Moy, V. T. & Gaub, H. E. (1994). Adhesion between individual ligand receptor pairs. *Science* **264,** 415–417.

Florin, E. L., Rief, M., Lehmann, H., Ludwig, M., Dornmair, C., Moy, V. T. & Gaub, H. E. (1995). Sensing specific molecular interactions with the atomic force microscope. *Biosensors Bioelectronics* **10,** 895–901.

Kasas, S., Thomson, N. H., Smith, B. L., Hansma, P. K., Miklossy, J. & Hansma, H. G. (1997). Biological applications of the AFM: from single molecules to organs. *Int. J. Imaging Syst. Tech.* **8,** 151–161.

Kellermayer, M. S. Z., Smith, S. B., Granzier, H. L. & Bustamante, C. (1997). Folding–unfolding transitions in single Titin molecules characterized with laser tweezers. *Science* **276,** 1112–1116.

Kramers, H. A. (1941). Brownian motion in a field of force and the diffusion model of chemical reaction. *Physica* **7,** 284–304.

Kuo, S. C. & Sheetz, M. P. (1993). Force of single kinesin molecules measured with optical tweezers. *Science* **260,** 232–234.

Lee, G. U., Chrisey, L. A. & Colton, R. J. (1994). Direct measurement of the forces between complementary strands of DNA. *Science* **266,** 771–773.

Ludwig, D., Jones, D. D. & Holling, C. S. (1978). Qualitative analysis of insect outbreak system: the spruce budworm and forest. *J. Anim. Ecol.* **47,** 315–332.

McQuarrie, D. A. (1976). *Statistical Mechanics*. New York: Harper & Rowe.

Meyerhofer, E. & Howard, J. (1995). The force generated by a single kinesin molecule against an elastic load. *Proc. Natl. Acad. Sci. U.S.A.* **92,** 574–578.

Moy, V. T., Florin, E. L. & Gaub, H. E. (1994). Intermolecular forces and energies between ligands and receptors. *Science* **266,** 257–259.

Murray, J. D. (1993). *Mathematical Biology*. New York: Springer-Verlag.

Nayfeh, A. H. & Balachandran, B. (1995). *Applied Nonlinear Dynamics*: *Analytical*, *Computational and Experimental Methods*. New York: Wiley.

Pethica, J. B. & Olver, W. C. (1987). Tip–surface interactions in STM and AFM. *Physica Scripta* **T19,** 61–66.

Rief, M., Gautel, M., Oesterhelt, F., Fernandez, J. & Gaub, H. (1997). Reversible unfolding of individual titin immunoglobulin domains by AFM. *Science* **276,** 1109–1112.

Rouse, P. E. (1953). A theory of the linear viscoelastic properties of dilute solution of coiling polymers. *J. Chem. Phys.* **21,** 1272–1280.

Sarid, D. (1991). *Scanning Probe Microscopy*. New York: Oxford.

Shapiro, B. E. & Qian, H. (1997). A quantitative analysis of single protein-ligand complex separation with the atomic force microscope. *Biophys. Chem.* **67,** 211–219.

Smith, S. B., Finzi, L. & Bustamante, C. (1992). Direct mechanical measurement of the elasticity of single DNA molecules by using magnetic beads. *Science* **258,** 1122–1126.

Tskhovrebova, L., Trinick, J., Sleep, J. A. & Simmons, R. M. (1997). Elasticity and unfolding of single molecules of the giant muscle protein titin. *Nature* **387,** 308–312.

Zimm, B. H. (1956). Dynamics of polymer molecules in dilute solution: viscoelasticity, flow birefringence and dielectric loss. *J. Chem. Phys.* **24,** 269–278.